

IMPROVED DETERMINATION OF THE ATMOSPHERIC PARAMETERS OF THE PULSATING SDB STAR FEIGE 48

M. LATOUR¹, G. FONTAINE¹, E.M. GREEN², P. BRASSARD¹, AND P. CHAYER³

Draft version July 3, 2021

ABSTRACT

As part of a multifaceted effort to exploit better the asteroseismological potential of the pulsating sdB star Feige 48, we present an improved spectroscopic analysis of that star based on new grids of NLTE, fully line-blanketed model atmospheres. To that end, we gathered four high S/N time-averaged optical spectra of varying spectral resolution from 1.0 Å to 8.7 Å, and we made use of the results of four independent studies to fix the abundances of the most important metals in the atmosphere of Feige 48. The mean atmospheric parameters we obtained from our four spectra of Feige 48 are : $T_{\text{eff}} = 29,850 \pm 60$ K, $\log g = 5.46 \pm 0.01$, and $\log N(\text{He})/N(\text{H}) = -2.88 \pm 0.02$. We also modeled for the first time the He II line at 1640 Å from the STIS archive spectrum of the star and we found with this line an effective temperature and a surface gravity that match well the values obtained with the optical data. With some fine tuning of the abundances of the metals visible in the optical domain we were able to achieve a very good agreement between our best available spectrum and our best-fitting synthetic one. Our derived atmospheric parameters for Feige 48 are in rather good agreement with previous estimates based on less sophisticated models. This underlines the relatively small effects of the NLTE approach combined with line blanketing in the atmosphere of this particular star, implying that the current estimates of the atmospheric parameters of Feige 48 are reliable and secure.

Keywords: stars : atmospheres — stars : fundamental parameters — stars : individual (Feige 48) — subdwarfs

1. INTRODUCTION

Koen et al. (1998) first reported the discovery of short-period (340-380 s) pulsations in the hot B subdwarf (sdB) star Feige 48. Since then, that star has attracted attention because it is relatively bright ($V = 13.48$) for a pulsator of the kind, and because its optical light curve shows relatively large pulsation amplitudes that may reach a few percent of the mean intensity of the star. This made it an ideal candidate for follow-up studies aimed at ultimately exploiting its full asteroseismic potential.

As a pulsator, Feige 48 was identified by Koen et al. (1998) to the then newly-found short-period p -mode oscillators of the EC 14026 type discovered shortly before (Kilkenny et al. 1997; Koen et al. 1997; Stobie et al. 1997; O’Donoghue et al. 1997). Interestingly, the existence of this class of pulsators had been predicted independently by theory (Charpinet et al. 1996, 1997). These pulsators are now officially known as V361 Hya stars, and informally referred to as sdB_r stars (Kilkenny et al. 2010). There exists another category of pulsating sdB’s, the long-period g -mode pulsators of the V1093 type (or sdB_s) discovered by Green et al. (2003). Fontaine et al. (2003) showed that the same basic process, a κ -mechanism fed by radiative levitation of iron-peak elements, is responsible for the excitation of pulsation modes in both types of pulsating hot B subdwarfs. Feige 48 finds itself at the common boundary between

the hotter, higher gravity sdB_r stars and the cooler, less compact sdB_s pulsators in the $\log g$ - T_{eff} diagram (see, e.g., Fig. 1 of Charpinet et al. 2013).

These two families of pulsating hot subdwarf stars show strong similarities with the pair β -Cephei / Slowly Pulsating Blue stars on the main sequence. However, sdB’s are evolved stars that lie well below the main sequence in the Hertzsprung-Russell diagram on the so-called Extreme Horizontal Branch. They are hot ($22,000$ K $\leq T_{\text{eff}} \leq 38,000$ K), compact ($5.2 \leq \log g \leq 6.2$) core helium burning objects. The hot B subdwarf stars are also chemically peculiar, showing strong He deficiencies and unusual metal abundance patterns (see, e.g., Geier 2013). Heber (2009) provides a comprehensive review of the properties of these intrinsically interesting, but still often neglected stars.

On the asteroseismological front, follow-up photometric observations gathered by Reed et al. (2004) with small telescopes over a period of five years confirmed the initial detection of five pulsation modes in Feige 48 as reported by Koen et al. (1998). Independent observations obtained at the Canada-France-Hawaii Telescope (CFHT) using the Montréal 3-channel photometer LAPOUNE produced a significant improvement of sensitivity leading to the uncovering of nine distinct pulsation modes, including the five previously known (Charpinet et al. 2005a). These modes were found to belong to four multiplet structures (two triplets, one doublet, and one singlet) associated with rotational splitting. For comparison with nonrotating models, only the four central periods of these complexes could be used, however. On this basis, Charpinet et al. (2005a) presented a preliminary seismic model of Feige 48 following the forward method developed by Brassard et al. (2001).

¹ Département de Physique, Université de Montréal, Succ. Centre-Ville, C.P. 6128, Montréal, QC H3C 3J7, Canada

² Steward Observatory, University of Arizona, 933 North Cherry Avenue, Tucson, AZ 85721

³ Space Telescope Science Institute, 3700 San Martin Drive, Baltimore, MD 21218

By incorporating rotation at the outset in their models, Van Grootel et al. (2008) were able to make full use of the nine distinct pulsation modes previously detected in the CFHT/LAPOUNE campaign and infer part of the internal rotation profile of Feige 48. This was used to test in a preliminary way spin-orbit synchronism in the close binary system that Feige 48 belongs to. Indeed, using HST/STIS observations and archive FUSE data, O’Toole et al. (2004) had previously found that Feige 48 is a member of such a system, with an orbital period of about 9 h. According to these authors, the unseen companion is likely a white dwarf, although the hypothesis of a cool main sequence star could not be completely ruled out.

Given the intrinsic importance of testing spin-orbit synchronism in close binary systems in general, we decided to exploit further the opportunity offered by the Feige 48 system. To this end, we first invested in a major white light photometric campaign from the ground, with the main objective of detecting many more pulsation modes than the nine uncovered previously. We were able to gather nearly 400 h of very high S/N data using the Mont4K camera attached to the Kuiper Telescope of the Steward Observatory Mount Bigelow Station. This was highly successful as some 46 pulsation modes were detected in Feige 48. Details will be reported elsewhere by Green et al. (in preparation).

As an integral part of these efforts, which will culminate with a new detailed seismic analysis of Feige 48 (Van Grootel et al., in preparation), we have pursued a spectroscopic campaign to obtain accurate radial velocity measurements and high S/N time-averaged spectra. The latter were used to obtain a more accurate determination of the atmospheric parameters of Feige 48, and this is what we report in this paper. As shown specifically in both Charpinet et al. (2005a) and Van Grootel et al. (2008), independent estimates of the atmospheric parameters of the pulsator – as provided by spectroscopy coupled to model atmosphere calculations – have been necessary to lift degeneracies in seismic solutions. This operation was then deemed crucial to our present multipronged efforts to understand better Feige 48 as a pulsator. We briefly review below what has been done in the past in terms of atmospheric analyses of the sdB star Feige 48, and we present the results of our own efforts based on the combination of the NLTE approach with the inclusion of detailed metal line blanketing in the atmosphere models.

2. SOME BACKGROUND

Hot subdwarf stars span a wide range of effective temperatures, from around 22,000 K for the coolest sdB’s to almost 100,000 K in the hottest sdO’s. Depending on the effective temperature, model atmospheres of varying sophistication need to be used in order to determine in a reliable way the atmospheric parameters and chemical composition of a hot subdwarf. For sdO stars, it has been shown that model atmospheres using the local thermodynamic equilibrium (LTE) approximation fail to reproduce observed spectra and lead to incorrect atmospheric parameters when one tries to fit the observed Balmer and helium lines with this type of model. In these stars, the non-LTE (NLTE) effects are undeniably important and must be taken into account when modeling their atmospheric layers. On the other hand, for

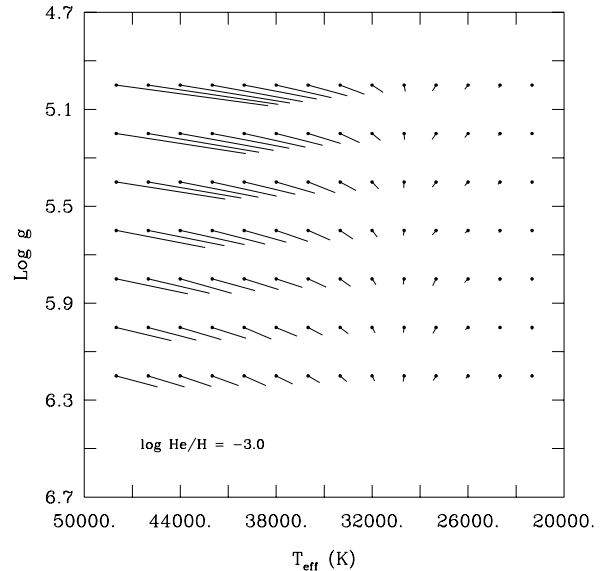


Figure 1. NLTE effects in the $\log g$ - T_{eff} plane. The dots give the original values of the atmospheric parameters for NLTE models with $\log N(\text{He})/N(\text{H}) = -3.0$ and no metals. The opposite end of each vector indicates the fictitious values of these parameters when the original spectra (treated as observational data) are analyzed with a grid of LTE models (again with no metals).

the coolest sdB stars, the LTE approximation usually gives correct results in terms of atmospheric parameters. The NLTE effects begin to be nonnegligible in the hottest sdB’s with effective temperatures around and beyond 30,000 K, which is also the temperature where He II lines become visible in the optical spectra (Napiwotzki 1997). For these hot sdB’s (sometimes referred to as sdOB stars), it becomes difficult to reproduce simultaneously both the He I and II lines, as is the case, for example, of the star PG 1219+534 where both LTE and NLTE approaches with metal-free models fail to reproduce helium lines from both ionization stages (Heber et al. 2000 and Charpinet et al. 2005b).

The situation concerning the importance of NLTE effects in sdB stars is, in fact, more complicated than the simple rule of thumb proposed by Napiwotzki (1997), namely, that these effects are negligible below $T_{\text{eff}} \sim 30,000$ K. There is also a dependency on the surface gravity and on the helium content. Figure 1 illustrates the results of analyzing a grid of synthetic spectra computed from metal-free NLTE models and treated as “observational” data, with a grid of theoretical spectra based on a similar grid of metal-free models, but computed, this time, in the LTE approximation. The helium abundance in this diagram refers to a value close to that found in Feige 48 (see below). The dots indicate the original values of the parameters of the NLTE models, while the end of each line segment indicates the fake values of these parameters as inferred with the LTE models. As expected, the largest deviations occur for the hotter and less compact atmospheres. And while it is true that the magnitude of the NLTE vectors becomes relatively small below $T_{\text{eff}} \sim 30,000$ K, the behavior is complex and not simply monotonic as revealed by the “rotating” vectors.

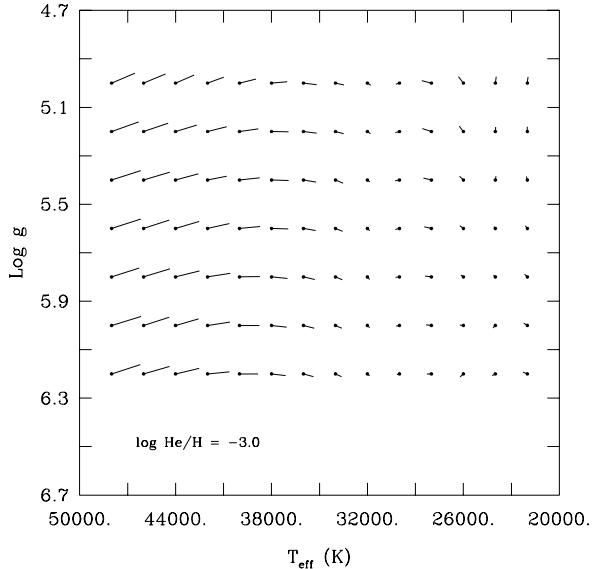


Figure 2. Metal blanketing effects in the $\log g$ - T_{eff} plane. The dots give the original values of the atmospheric parameters for NLTE models with $\log N(\text{He})/N(\text{H}) = -3.0$ and a metallicity specified by C(0.1 solar), N(solar), O(0.1 solar), Si (0.1 solar), S(solar), and Fe(solar). The opposite end of each vector indicates the fictitious values of these parameters when the original spectra (treated as observational data) are analyzed with a grid of NLTE models with no metals.

Another important ingredient in atmosphere modeling are the metallic elements that cause line blanketing and thus change the shape of the spectral energy distribution of the star. Changes in the emergent spectrum are more important in the UV domain and at shorter wavelengths where a large number of absorption lines, mainly from iron-peak elements, block an important fraction of the flux. The flux must nevertheless come out of the star, and it does so at larger wavelengths, increasing the continuum level of these regions. The line blanketing caused by metals also has an effect on the thermodynamical structure of the atmosphere by heating the inner layers and cooling the outer ones. All of this has repercussions in the optical domain where the Balmer and helium lines used to determine the atmospheric parameters of a star are found. If these lines are affected by the presence of metallic elements, so will the atmospheric parameters derived by fitting them.

Adding elements heavier than helium into model atmospheres computed in the LTE approximation is now a common practice and LTE line-blanketed model atmospheres are often used to study sdB stars. As for NLTE models, including metals in them is a much more complicated task than doing it in their LTE counterparts. As a consequence, and to our knowledge, the only extensive and detailed grids of atmosphere models for sdB stars combining the NLTE approach with metals have been those of Brassard et al. (2010) and Németh et al. (2012). Figure 2 based on some of the models of Brassard et al. (2010) illustrates particularly well the effects of including C, N, O, Si, S, and Fe in NLTE calculations for sdB stars on the derived atmospheric parameters. Those elements are the most abundant metals that have been measured in a sample of five sdB_s stars by Blanchette et al.

(2008) on the basis of UV data from the Far-Ultraviolet Spectroscopic Explorer (FUSE), and their average abundances have been adopted as a representative metallicity in the NLTE calculations of Brassard et al. (2010). Given that previous estimates of the atmospheric parameters of Feige 48 have led to $T_{\text{eff}} \simeq 30,000$ K and $\log g \simeq 5.5$ (see below), one can anticipate from Figure 2 that the effects of metal line blanketing cannot be very large in the atmosphere of that star. Still, given the importance of Feige 48 as a pulsator in a close binary system, we have felt it worthwhile to carry out the present analysis using the state of the art models in the field.

3. SPECTRAL ANALYSIS OF FEIGE 48

3.1. Previous Studies

The first estimates of the atmospheric parameters of Feige 48 based on a spectroscopic analysis were obtained by Koen et al. (1998) when they found the star to be an EC 14026 pulsator. They used a grid of LTE model atmospheres with pure hydrogen, and this led to an effective temperature of $28,900 \pm 300$ K and a $\log g$ of 5.45 ± 0.05 . Later, Heber et al. (2000) revised these values a bit upward with their detailed analysis of a Keck/HIRES spectrum of Feige 48. They derived atmospheric parameters by fitting the Balmer and He I lines with three kinds of models: LTE with a solar metallicity, metal-poor LTE with $[M/H] = -2.0$, and NLTE without metals (H and He only). Their temperature estimates agreed well with each other, and they were slightly higher than the one found by Koen et al. (1998). Taking the mean value of their three estimates and the one from Koen et al. (1998), they finally adopted $29,500 \pm 350$ K as the effective temperature of Feige 48. Their values of $\log g$ obtained with the three types of models are similar, and using the same approach as they did for the temperature, Heber et al. (2000) got a mean $\log g$ of 5.50 ± 0.05 . Finally, the helium abundance was basically also the same for each type of models, and they got a final value of $\log N(\text{He})/N(\text{H}) = -2.93 \pm 0.05$. Note that the Keck/HIRES data allowed Heber et al. (2000) to constrain the projected rotational velocity of Feige 48 to $v_{\text{rot}} \sin i \leq 5$ km s⁻¹, thus indicating that the star is a relatively slow rotator or an object seen nearly pole-on, or both.

When Feige 48 was studied from an asteroseismological point of view by Charpinet et al. (2005a), these authors also obtained a new, independent derivation of its atmospheric parameters. Charpinet et al. (2005a) combined a high S/N, medium resolution (~ 1 Å) spectrum that they gathered at the MMT with a grid of metal-free H,He NLTE model atmospheres, obtaining $T_{\text{eff}} = 29,580 \pm 370$ K, $\log g = 5.48 \pm 0.05$, and $\log N(\text{He})/N(\text{H}) = -2.95 \pm 0.08$. Their asteroseismic analysis confirmed the spectroscopic value of the gravity with a best match at $\log g = 5.44$. Hence, according to the previous available spectroscopic analyses, the atmospheric parameters of Feige 48 seem to be well constrained and do not show an important dependence on either the type of model atmospheres (LTE or NLTE) or the presence of metallic elements in LTE models.

In the past few years, we developed an efficient way of computing NLTE line-blanketed model atmospheres using versions of the public codes TLUSTY and SYNSPEC

(Lanz & Hubeny 1995, 2003a, 2007) running on a cluster of dedicated PC's that now include 320 processors (see Latour et al. 2011 for more details on the setup). More than 300 model atmospheres can thus be computed at the same time. This made it straightforward for us to use this more sophisticated approach for modeling the atmosphere of Feige 48. This allows for exploiting at their full potential the spectroscopic data that we gathered on Feige 48, and for supporting its forthcoming seismic analysis with the most accurate atmospheric parameters that can be currently obtained.

3.2. Observational Material

We have at our disposal four optical spectra of Feige 48, spanning different wavelength ranges and having different resolutions. Our best data set is a combination of medium resolution (1 Å) spectra acquired between 2002 and 2013 with the blue spectrograph attached to the 6.5 m Multiple Mirror Telescope (MMT). This was part of the ongoing radial velocity program on sdB stars carried out by one of us (E.M.G.). Throughout the observing seasons, the same experimental setup was consistently used. The 832 mm⁻¹ grating in second order and 1" slit provide a resolution R of ~ 4250 (1.05 Å) over the wavelength range 4000–4950 Å. The slit was always aligned at the parallactic angle during the observations. Exposures of 240 to 475 s, depending on conditions, resulted in signal-to-noise ratios (S/N) of about 80 to 150 for individual spectra, which is sufficient to achieve velocity errors of 1 to 2 km s⁻¹ for sdB stars. One to four spectra per night were obtained. The spectrum used for the present spectroscopic analysis is the combination of 17 mean nightly spectra gathered during different runs, median-filtered and shifted to the same velocity prior to combining. Thus the resulting spectrum has a remarkably high formal S/N of ~ 460 . This spectrum will be referred to as MMT. We point out that an earlier, reduced sensitivity version of this spectrum was used by Charpinet et al. (2005a) in their seismic analysis.

Our second spectrum is also a medium-resolution one obtained from the combination of several individual spectra gathered over the last several years within the context of the radial velocity program of E.M.G. carried out on sdB stars. These data were obtained with the Boller & Chivens (B&C) Cassegrain spectrograph at Steward Observatory's 2.3 m Bok Telescope on Kitt Peak. The 832 mm⁻¹ grating in second order with a 1.5" slit were used to achieve 1.9 Å resolution over a wavelength range of 3675–4520 Å. The slit was aligned with the parallactic angle at the midpoint of each exposure, and comparison HeAr spectra were taken before and after each stellar spectrum. Exposure times between 500 and 875 s for the individual spectra led to S/N of about 50 to 80. The final spectrum is the combination of 50 exposures and has a resulting S/N of ~ 375 . This spectrum will be referred to as BG2 (as in "Betsy Green's ~ 2 Å spectrum").

Another spectrum of Feige 48 was kindly gathered for us by Pierre Bergeron using again the B&C spectrograph on the 2.3 m Bok telescope. This was part of a request to observe for us several pulsating sdB stars during two of his white dwarf observing runs going back to 2006. In that case, the 4.5" slit together with the 600 mm⁻¹ grating blazed at 3568 Å in first order provided a spectral

coverage from about 3030 to 5250 Å at a resolution of ~ 6.0 Å. The S/N of this single spectrum is ~ 80 . Even though this spectrum is of lower quality than the previous ones in terms of sensitivity and resolution, we felt that it would be worthwhile to analyze all spectral data available to us on our target star. This third spectrum is referred to as PB6 in what follows.

Finally, we have at our disposal an older (2004) high-sensitivity, low-resolution spectrum of Feige 48 gathered again with the B&C spectrograph on the 2.3 m Bok telescope. It is the combination of 5 exposures using the 400 mm⁻¹ grating in first order in conjunction with a 2.5" slit to obtain a typical resolution of 8.7 Å over the wavelength interval 3620–6900 Å, thus including H α . The instrument rotator was set prior to each exposure, to align the slit within $\sim 2^\circ$ of the parallactic angle at the midpoint of the exposure. HeAr comparison spectra were obtained immediately following each stellar exposure. The blue part of the combined spectrum reaches S/N $\simeq 248$. This spectrum is to be referred to as BG9. It was used previously by Charpinet et al. (2005a) in their analysis of Feige 48.

Inspection of our optical data revealed no sign of He II lines in the spectra. There is also no hint for the presence of He II $\lambda 4686$ or other weaker features associated with that ionization stage in the high-resolution HIRES spectrum of Feige 48 obtained by Heber et al. (2000). However, since Feige 48 has been observed with the STIS spectrograph and these data are available in the Mikulski Archive for Space Telescopes (MAST)⁴, we checked the UV spectrum in order to verify if the strongest expected He II feature in that wavelength range, the $\lambda 1640$ line, could be detected (see O'Toole & Heber 2006 for more details on the data). Indeed, the line is present, although somewhat weak and noisy, but it is still sufficiently useful as the sole indicator of that ionization stage of helium to provide us below with a nice test of the validity of our derived atmospheric parameters based on the optical data.

3.3. Model Atmospheres

3.3.1. The Metallicity of Feige 48

In order to fix a suitable chemical composition for the grid of models, we searched the literature for abundance studies done on Feige 48. Because of its status of pulsating star and its brightness, Feige 48 has been thoroughly studied and its atmospheric chemical composition has been analyzed in at least four different studies that we know of. First, after their determination of the atmospheric parameters of the star on the basis of a HIRES spectrum, Heber et al. (2000) carried out an abundance analysis of visible metals and found the star to have sub-solar abundances for all of the eight elements they studied, except for iron which was found to be solar. For their part, Chayer et al. (2004) made a comparison of the chemical composition of Feige 48 and Feige 87 (a non-variable sdB with atmospheric parameters very similar to those of Feige 48) using UV metallic lines present in the star's FUSE spectrum. O'Toole & Heber (2006) also undertook an abundance analysis of a sample of pulsating and constant sdB stars (among them Feige 48) in order

⁴ <http://archive.stsci.edu/>

Table 1
Abundances of Metals Detected in the Atmosphere of Feige 48 : $\log N(Z)/N(H)$

Element Z	Heber et al. (2000) Keck/HIRES	Chayer et al. (2004) <i>FUSE</i>	O'Toole & Heber (2006) <i>HST/STIS</i>	Geier (2013) Keck/HIRES	Mean	This work MMT	Solar ^a
C	-4.64±0.03	-5.2±0.5	-4.79±0.10	-4.65±0.35	-4.65±0.03	-4.94±0.1	-3.57
N	-4.29±0.10	-4.6±0.5	-4.38±0.38	-4.72±0.12	-4.47±0.07	-4.61±0.2	-4.17
O	-4.21±0.12	< -4.2	...	-4.35±0.20	-4.25±0.10	-4.47±0.1	-3.31
Ne	-4.90±0.31	< -4.06	-4.90±0.31	...	-4.07
Mg	-5.09±0.50	-5.2±0.50	-5.15±0.35	-5.18±0.2	-4.40
Al	-5.50±0.18	< -5.8	-6.49±0.10	-6.4±0.5	-6.49±0.09	...	-5.55
Si	-5.67±0.27	-5.7±0.5	-5.73±0.19	-5.45±0.06	-5.49±0.06	-5.38±0.3	-4.49
P	...	-7.1±0.5	-7.59±0.50	< -7.02	-7.35±0.35	...	-6.59
S	-5.85±0.50	-5.7±0.5	...	-6.05±0.07	-6.04±0.07	-5.71±0.3	-4.88
Cl	...	< -8.5	< -8.5	...	-6.50
Ar	...	< -6.8	< -5.0	< -5.18	< -6.8	...	-5.60
K	< -6.07	< -6.07	...	-6.97
Ca	-4.69±0.50	...	-4.69±0.50	...	-5.66
Sc	< -9.0	...	< -9.0	...	-8.85
Ti	...	< -7.6	-6.81±0.13	< -6.26	-6.81±0.13	...	-7.05
V	...	< -8.3	...	< -5.03	< -8.3	...	-8.07
Cr	...	-7.0±0.5	-5.95±0.15	...	-6.04±0.14	...	-6.36
Mn	...	-7.0±0.5	-6.38±0.21	...	-6.47±0.19	...	-6.57
Fe	-4.45±0.19	-4.8±0.5	-4.30±0.14	-4.54±0.21	-4.41±0.10	-4.48±0.2	-4.50
Co	...	-7.6±0.5	-6.11±0.18	...	-6.28±0.17	...	-7.01
Ni	...	< -5.7	-5.31±0.15	...	-5.31±0.15	...	-5.78
Cu	-6.75±0.40	...	-6.75±0.40	...	-7.81
Zn	-6.70±0.22	...	-6.70±0.22	...	-7.44
Ga	-7.30±0.50	...	-7.30±0.50	...	-8.96
Ge	-7.98±0.08	...	-7.98±0.08	...	-8.35
Sn	-9.06±0.50	...	-9.06±0.50	...	-9.96
Pb	-8.20±0.50	...	-8.20±0.50	...	-10.25

^a Asplund et al. (2009)

to test the hypothesis that pulsating sdB's might show a different abundance pattern than the nonpulsating ones. This was not the case, but they nevertheless got a rather good picture of the abundance patterns in the five stars they studied. Finally, in an attempt to go further into deriving general trends for the metallic abundances in sdB stars, Geier (2013) analyzed a much larger sample of sdB's (among them Feige 48) using high-resolution optical spectra. Among other results, he obtained a fourth set of metal abundances for the star of interest.

Table 1 reports our compilation of the abundances obtained in the four previously mentioned studies. A weighted mean abundance was computed for each element, and since the uncertainty is used as weight, we attributed a value of ± 0.5 dex whenever there was no uncertainty quoted in the reference paper. We included in our model grid the mean abundance of the eight metals that are indicated in bold in Table 1. We limited ourselves to the inclusion of ten atomic species (including H and He) in our models, for stability and convergence reasons. Therefore, we chose to include the eight most abundant metallic species, except for calcium which we left aside because its abundance is based on a single optical line. This table also features (7th column) the abundances that we derived using the MMT spectra (see Section 3.5 below).

It is worth mentioning that Heber et al. (2000), O'Toole & Heber (2006), and Geier (2013) used the following parameters for their abundance analyses: $T_{\text{eff}} = 29,500$ K, $\log g = 5.54$, and $\log N(\text{He})/N(\text{H}) = -2.9$. The remaining study of Chayer et al. (2004) used parameters quite similar. O'Toole & Heber (2006) used line-blanketed LTE model atmospheres with solar metallicity. Otherwise, the three other studies also used LTE mod-

els (although it is not clearly mentioned in Heber et al. 2000) with a certain amount of metallic elements that was not explicitly mentioned.

3.3.2. Model Grids

Having determined in Table 1 the metallicity to be included in our models, we first built a small grid of 150 NLTE line-blanketed model atmospheres especially suited for Feige 48. The grid includes 5 values of T_{eff} between 26,000 K and 34,000 K in steps of 2000 K, 6 values of $\log g$ between 5.0 and 6.0 in steps of 0.2 dex, and 5 helium abundances between $\log N(\text{He})/N(\text{H}) = -4.0$ and -2.0 in steps of 0.5 dex. Our models contains the following species: H, He, C, N, O, Ne, Mg, Si, Fe, and Ni. The main characteristics of the model atoms used are listed in Table 2. The population of each level and superlevel is computed in NLTE and the number of lines correspond to the allowed transitions between these levels and superlevels. Model atoms of iron and nickel are built in a different way than the lighter elements: all the NLTE levels are in fact superlevels and each of them includes a certain number of individual levels. The populations of individual levels inside a superlevel are computed assuming a Boltzmann distribution. The number of line transitions indicated for iron and nickel are those occurring between the individual levels. Further technical details on the atomic data used in TLUSTY can be found in Lanz & Hubeny (2003b). The highest ionization stage of each element is taken as a one-level atom. Most of the models we used are available on the TLUSTY web page⁵.

Before performing the fitting procedure on the spectra

⁵ <http://nova.astro.umd.edu/Tlusty2002/tlusty-frames-data.html>

Table 2
Details of the model atoms used in our model atmospheres

Ion	No. of levels/superlevels	No. of lines ^a
H I	8/1	30
He I	19/5	104
He II	20/-	121
C II	17/5	105
C III	34/12	380
C IV	21/4	150
C V	1	-
N II	32/10	278
N III	25/7	184
N IV	34/14	384
N V	10/6	86
N VI	1	-
O II	36/12	346
O III	28/13	224
O IV	31/8	270
O V	34/6	222
O VI	1	-
Ne I	23/12	219
Ne II	23/9	178
Ne III	12/2	20
Ne IV	10/2	22
Ne V	1	-
Mg I	12/6	56
Mg II	21/4	146
Mg III	1	-
Si II	13/3	48
Si III	31/15	341
Si IV	19/4	130
Si V	1	-
	No. of levels NLTE/LTE	No. of lines ^b
Fe II	36/10921	1264969
Fe III	50/12660	1604934
Fe IV	43/13705	1776984
Fe V	42/11989	1008385
Fe VI	1	-
Ni III	36/11335	1309729
Ni IV	38/13172	1918070
Ni V	48/13184	1971819
Ni VI	1	-

^a Allowed transitions

^b Transitions between LTE levels

of Feige 48, we examined a few properties of our models. We first looked at the differences produced on the temperature structure by the metallic elements included in the atmosphere as compared to the metal-free case. Figure 3 shows the temperature structures for four model atmospheres having the same parameters ($T_{\text{eff}} = 30,000$ K, $\log g = 5.4$, and $\log N(\text{He})/N(\text{H}) = -3.0$), except for their metallicity. The black curve is from a model including only hydrogen and helium, showing the typical NLTE temperature inversion in the upper layers of a metal-free atmosphere. The red curve illustrates the case where only our six “lighter” metals were included in the calculations. Their main effect is to cool down the upper layers. The most noteworthy effect of adding iron (green curve) is the concomitant back-warming of the deeper layers, which results in a higher temperature at a given depth. We also included the temperature profile (blue curve) of a fully line-blanketed model which includes all of the eight metallic elements. The only difference between the blue and the green curves is the addition of nickel and it can be seen that, at least for a model representing Feige 48, the influence of this element on the thermodynamical structure of the model remains rather

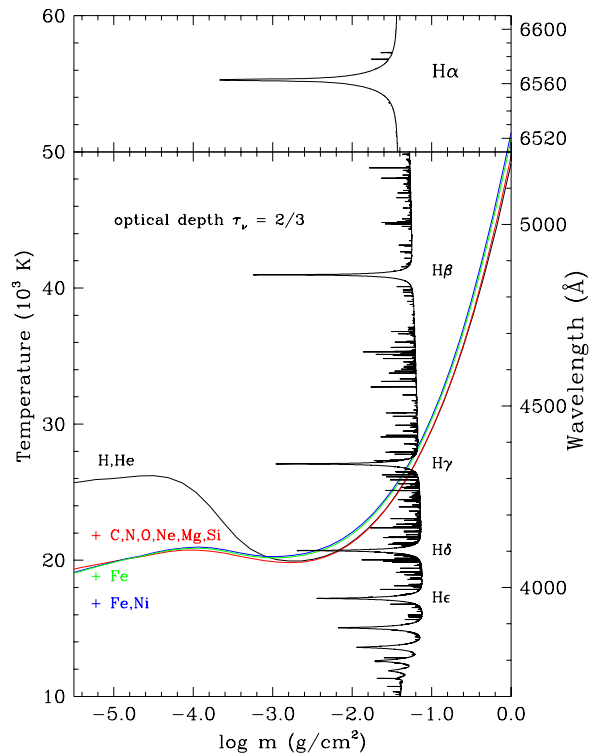


Figure 3. Temperature stratification and monochromatic optical depth $\tau_\nu = 2/3$ as functions of depth, where m is the column density, for NLTE models defined by $T_{\text{eff}} = 30,000$ K, $\log g = 5.4$, and $\log N(\text{He})/N(\text{H}) = -3.0$. The temperature structure is shown for four model atmospheres having different compositions : with H and He only (black), with C, N, O, Ne, Mg, Si in addition (red), with Fe added to the previously mentioned elements (green), and finally with Ni on top of that (blue). The $\tau_\nu = 2/3$ curve is from the latter model and shows wavelength intervals corresponding to the Balmer line series.

small. Overall, the line-blanketing effects are qualitatively the same as what is seen in model atmospheres at higher temperature (for sdO stars), but to a lesser extent. The drop in the surface temperature is around 7,000 K for our Feige 48 models, while it can be around 40,000 K in 80,000 K sdO models (see, e.g., Fig. 1 of Latour et al. 2013). In the deeper layers ($\log m \gtrsim -3.0$), the rise of the temperature due to the metals is around four percent. Also featured in Figure 3 is the optical depth $\tau_\nu = 2/3$ as a function of the column density (m), allowing one to infer where, in the atmosphere, the Balmer and metallic lines as well as the continuum are formed.

We also wanted to verify how these changes in the structure of our models might affect the computed optical spectrum and, by extension, any derived atmospheric parameters. To illustrate this, we created the map featured in Figure 4. This is similar to our Figure 2 above, but specialized to the specific metallicity used to model Feige 48. To construct this map, spectra from one grid of models are considered as “observed” spectra and are fitted with a different grid of synthetic spectra. We performed our fitting procedure in the 4020–4910 Å interval, which includes three Balmer lines and four He I lines, with mod-

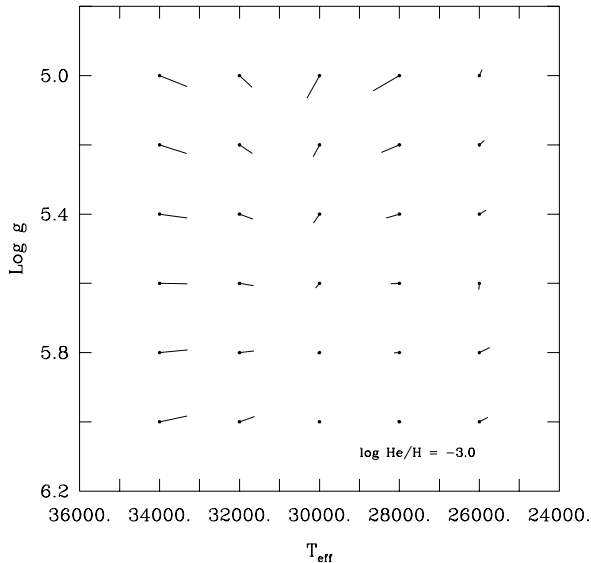


Figure 4. Map illustrating the effects of metal line blanketing on the inferred atmospheric parameters. T_{eff} and $\log g$ are obtained for some models of our NLTE line-blanketed grid fitted with a grid of NLTE H,He models. The atmospheric parameters of the models are indicated by dots while the end of line segments correspond to the parameters obtained by the fitting procedure. The helium abundance is kept fixed at the model value of $\log N(\text{He})/N(\text{H}) = -3.0$.

els convolved at 1 \AA resolution in order to mimic the MMT spectrum. Because we wanted to check the effects of line blanketing, spectra from our fully-blanketed grid were taken as the observed ones and we fitted them with a grid of theoretical spectra obtained with model atmospheres including only hydrogen and helium. Our χ^2 fits were done in order to derive an optimal solution in terms of effective temperature and surface gravity, while the helium abundance was kept fixed at its real value. Figure 4 shows our results for a helium abundance similar to the one found in Feige 48 ($\log N(\text{He})/N(\text{H}) = -3.0$). We can see, once again and in complement to Figure 2, that the effects of metals on the derived atmospheric parameters remain small throughout the domain investigated. Somewhat accidentally in the specific case of Feige 48 with $T_{\text{eff}} \simeq 30,000 \text{ K}$ and $\log g \simeq 5.5$, the effects are particularly small.

3.4. Derived Atmospheric Parameters

We analyzed the four spectra with both our fully-blanketed model grid and a more classic metal-free NLTE, H,He grid that was also computed as indicated just above. We used a χ^2 minimization procedure similar to that of Saffer et al. (1994). A simultaneous fit of the Balmer and helium lines available in our spectra was carried out in order to find the optimal solution in the three-dimensional space defined by the parameters T_{eff} , $\log g$, and $\log N(\text{He})/N(\text{H})$. Prior to that exercise, all the synthetic spectra (defined by 32001 wavelength points in the range $3500\text{--}6700 \text{ \AA}$) were degraded by convolution to the experimental resolution of each of the available spectrum of Feige 48. We note that microturbulence is a nonissue here given the resolutions of our optical spectra. The four panels of Figure 5 show our resulting fits

when using the fully-blanketed grid described in the previous subsection. Panel a) shows the results achieved for the MMT spectrum, Panel b) for the BG2 spectrum, Panel c) for the PB6 spectrum, and Panel d) for the BG9 spectrum. The results of these fits, as well as the ones obtained with the H,He grid, are also reported in Table 3. Note that the quoted uncertainties only reflect the quality of the fits; they are formal fitting errors.

When examining the resulting T_{eff} and $\log g$ entries for both grids in Table 3, one can notice a small systematic trend in the determined values: from top (MMT) to bottom (BG9), with decreasing resolution, both the derived effective temperature and the surface gravity increase slightly. The differences are not large (at most 600 K and $\sim 0.09 \text{ dex}$), but the trend is nevertheless noticeable. However, the resolution is not the only difference between the four spectra; the spectral range also varies and, thus, the lines featured and fitted in each spectrum are not the same. Hence, the differences in the fitted spectral range could very well affect the resulting parameters in a systematic way. In order to check the effects of varying the spectral range, we carried out some additional fits with the two lowest resolution spectra. We thus fitted the BG9 spectrum over the reduced spectral ranges of the MMT, BG2, and PB6 spectra, and the PB6 spectrum over the MMT and BG2 ranges. The results are shown in Table 3 below the weighted mean values of the four “conventional” fits for the two different grids. It should be mentioned here that our fits usually start at 3740 \AA (just to the red of the H12 line), except for the MMT spectrum whose blue limit is at 4000 \AA .

From Table 3, one can realize that the inferred parameters (effective temperature, surface gravity, helium abundance) are essentially the same for the four different spectral ranges considered when using the BG9 spectrum. And indeed, the derived values are the same within the formal fitting errors, and this is the case for both types of model grids as well. This is true also for the three different spectral ranges used in conjunction with the PB6 spectrum. We thus conclude that, at low enough resolution, no significant systematic trend is associated with the choice of the spectral range. On the other hand, resolution does matter here as can be seen by comparing the derived parameters obtained with the MMT spectrum, the PB6 spectrum fitted over the MMT range only, and the BG9 spectrum again fitted over the MMT range only. Although the formal uncertainties overlap between the MMT and PB6+MMT cases, there is indeed a small but significant trend such that the effective temperature and the surface gravity increase slightly with decreasing resolution as can be inferred by comparing the MMT and BG9+MMT cases. For its part, the helium abundance is essentially unchanged as a function of resolution taking into account the formal errors of the fits. A final look at the effects of changing the resolution is provided by an experiment in which we degraded the resolution of the original MMT spectrum through convolution with a Gaussian with a FWHM of 8.7 \AA . The new inferred parameters using this degraded spectrum are $T_{\text{eff}} = 29,922 \pm 100 \text{ K}$, $\log g = 5.477 \pm 0.015$, and $\log N(\text{He})/N(\text{H}) = -2.805 \pm 0.025$, to be compared with the first line in Table 3 giving $T_{\text{eff}} = 29,674 \pm 106 \text{ K}$, $\log g = 5.429 \pm 0.016$, and $\log N(\text{He})/N(\text{H}) = -2.882 \pm 0.023$.

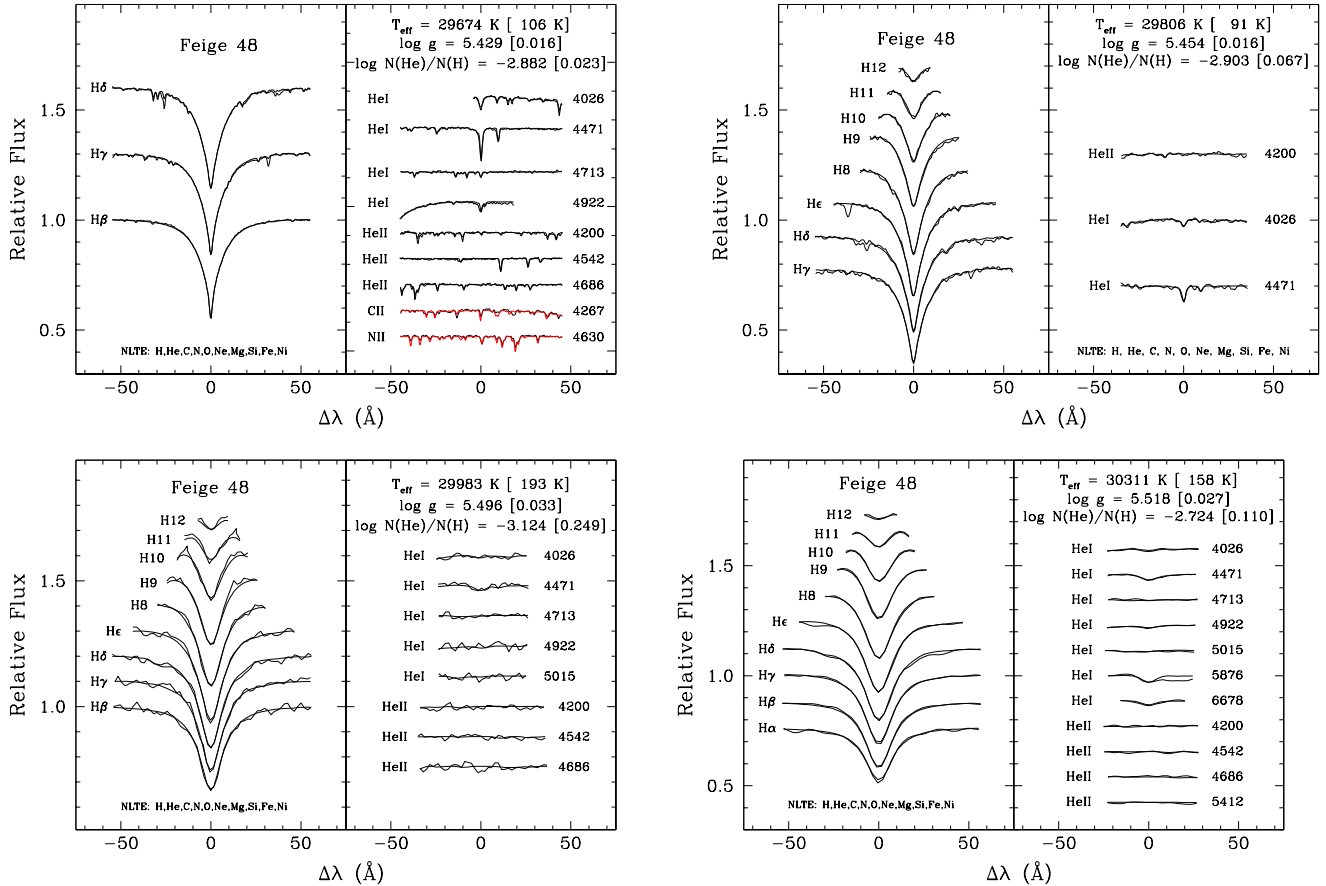


Figure 5. Top-left a) Best fit obtained with the 1 Å resolution MMT spectrum of Feige 48 using our grid of NLTE line-blanketed model atmospheres described in Subsection 3.3.2. The Balmer and He I lines are all very well reproduced by the optimal model. Top-right b) Same as (a) but with the bluer 1.9 Å resolution spectrum (BG2). Bottom-left c) Same as (a) but with the 6 Å resolution spectrum (PB6). Note that a sole line of He I at 4471 Å is discernible in this spectrum, which explains the lower helium abundance found (log $N(\text{He})/N(\text{H}) = -3.124$) and the larger error associated with this value. Bottom-right d) Same as (a) but this time with the lowest resolution spectrum (8.7 Å) BG9. In spite of its low resolution, the high S/N allows to distinguish three He I lines and guess the 4026 Å one.

Finally, comparing the atmospheric parameters obtained with the line-blanketed grid versus the H,He one, we note that adding metals to NLTE models leads to only slightly lower effective temperatures and surface gravities. This is exactly what Figure 4 above shows for the parameters appropriate for Feige 48. As for the effects on the helium abundance, they are completely negligible. Having done all those fits, we at last end up with the following atmospheric parameters for Feige 48: $T_{\text{eff}} = 29,854 \pm 60$ K, $\log g = 5.459 \pm 0.013$, and $\log N(\text{He})/N(\text{H}) = -2.880 \pm 0.021$. These are our best estimates, based on the weighted averages of the values obtained when fitting the four available spectra with the fully-blanketed grid of model atmospheres (the first four lines in Table 3). Of course, the quoted uncertainties only reflect the quality of the fits.

A potentially interesting test of our derived atmospheric parameters for Feige 48 is to attempt fitting the He II $\lambda 1640$ line detected in the UV and available in the MAST archives (see Section 3.2). This spectral feature is the only one corresponding to the He II ionization stage that is available for that star. Otherwise, there are no He II lines visible in the optical spectrum of Feige 48 because of its relatively low effective temperature and its

low helium abundance as determined just above. Our first attempt to fit the He II $\lambda 1640$ line in our standard three-dimensional search domain (T_{eff} , $\log g$ and $\log N(\text{He})/N(\text{H})$) would not converge to a unique solution, most likely because of the numerous metallic lines in the vicinity of the helium line. So we redid the exercise, this time keeping the helium abundance fixed to the value found previously (-2.88), and leaving the fitting procedure find the best match in terms of effective temperature and gravity only. The program did converge this time to a solution giving $T_{\text{eff}} = 30,450 \pm 930$ K and $\log g = 5.43 \pm 0.30$, which is perfectly consistent with our previous results. Even though the fitting errors for the sole He II $\lambda 1640$ line are larger than what was obtained with the whole visible spectra, we take this as a nice consistency check for the validity of our derived atmospheric parameters. The resulting fit is presented in Figure 6, where it is possible to see the He II line blended with Fe IV and Ni III lines around 1640 Å and other Fe IV lines in its red wing.

3.5. Fine Tuning of the Metal Abundances

Our MMT spectrum, because of its good resolution and excellent signal-to-noise ratio, features a lot of dis-

Table 3
Results of our fitting procedure for Feige 48

Spectrum	T_{eff} (K)	$\log g$ (dex)	$\log N(\text{He})/N(\text{H})$ (dex)	Note
With our NLTE fully line-blanketed model grid				
MMT	$29,674 \pm 106$	5.429 ± 0.016	-2.882 ± 0.023	
BG2	$29,806 \pm 91$	5.454 ± 0.016	-2.903 ± 0.067	
PB6	$29,983 \pm 193$	5.496 ± 0.033	-3.124 ± 0.249	
BG9	$30,311 \pm 158$	5.518 ± 0.027	-2.724 ± 0.110	
Mean	$29,854 \pm 60$	5.459 ± 0.013	-2.880 ± 0.021	
PB6	$30,010 \pm 169$	5.487 ± 0.035	-3.094 ± 0.256	with BG2
PB6	$29,765 \pm 639$	5.488 ± 0.093	-3.247 ± 0.290	with MMT
BG9	$30,264 \pm 113$	5.517 ± 0.020	-2.803 ± 0.101	with PB6
BG9	$30,220 \pm 130$	5.543 ± 0.024	-2.836 ± 0.128	with BG2
BG9	$30,483 \pm 384$	5.521 ± 0.057	-2.779 ± 0.099	with MMT
With our NLTE H,He model grid				
MMT	$29,840 \pm 141$	5.441 ± 0.024	-2.898 ± 0.032	
BG2	$30,013 \pm 83$	5.466 ± 0.016	-2.897 ± 0.068	
PB6	$30,161 \pm 167$	5.502 ± 0.033	-3.135 ± 0.259	
BG9	$30,520 \pm 130$	5.522 ± 0.027	-2.736 ± 0.107	
Mean	$30,105 \pm 59$	5.474 ± 0.011	-2.889 ± 0.028	
PB6	$30,182 \pm 173$	5.502 ± 0.035	-3.078 ± 0.258	with BG2
PB6	$29,879 \pm 561$	5.478 ± 0.094	-3.265 ± 0.321	with MMT
BG9	$30,493 \pm 101$	5.521 ± 0.021	-2.805 ± 0.105	with PB6
BG9	$30,455 \pm 112$	5.549 ± 0.025	-2.847 ± 0.131	with BG2
BG9	$30,694 \pm 340$	5.537 ± 0.063	-2.779 ± 0.111	with MMT

cernible metallic lines. When looking closely at our best-fit model shown in Figure 5a, it can be noticed that the lines of some elements are systematically stronger or fainter than the observed ones, thus calling for a bit of fine tuning in order to obtain a better match with the observations. So we fitted the elements whose lines are visible in the wavelength range of the MMT spectrum (4020–4950 Å), namely C, N, O, Mg, Si, S and Fe. These fits were done by using a model atmosphere having the atmospheric parameters determined by our fit of the MMT spectrum (first line in Table 3) and the chemical composition mentioned in Section 3.3.1 (with the exception of iron which was not included in the model atmosphere; see discussion below). Using this model, we computed several families of synthetic spectra with six or seven different abundances for each element analyzed. The abundance of the element was changed only in the computations of the emergent spectrum by SYNSPEC

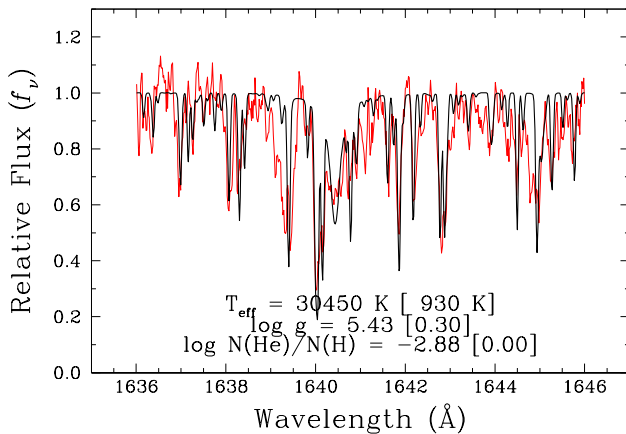


Figure 6. Our best fit of the He II $\lambda 1640$ line in the STIS spectrum of Feige 48 in terms of effective temperature and surface gravity.

(see the SYNSPEC user’s guide for more details⁶). This approach is not entirely self-consistent, but because the spectrum of Feige 48 turns out to be not much affected by line-blanketing nor NLTE effects, and also because we do not expect drastic changes in the abundances, we think this method is reasonable for this particular case.

The detailed comparison of the observed MMT spectrum with our final best synthetic one (having adjusted metal abundances) is shown in Figure 7. The original best-fit spectrum, seen in Figure 5a, is also featured in the comparison (dotted line). This way the improvement brought by the fine tuning can easily be seen. The new abundances obtained by fitting the metallic lines of the MMT spectra are indicated in Table 1. The uncertainties were obtained from the standard deviation of the abundances indicated by different lines of a same element, or by eye when only one line of the element was fitted. Specifically, we decreased by a few tenths of a dex the abundances of carbon, nitrogen, and oxygen. This resulted in a better agreement between the observed and synthetic spectrum for most of the lines originating from O II, N II, and the C II doublet at 4267 Å. The only noteworthy remaining discrepancies (after our adjustments) for these elements are the O II lines at 4075.8 Å that are still too strong. Magnesium and silicon kept roughly the same abundances we considered initially; in those cases, their lines were already well reproduced with our best-fit model. Sulfur was not included in the model atmospheres at the outset, but when added into the synthetic spectrum, its lines, including one blended with an O II line at our resolution, were better reproduced (see Figure 7b) with an abundance a bit higher than the mean one indicated in Table 1.

Finally, iron was a particular case. We noticed that most of the iron lines were too shallow in our optimal synthetic spectrum, and we were unable to obtain a good

⁶ <http://nova.astro.umd.edu/Tlusty2002/tlusty-frames-guides.html>

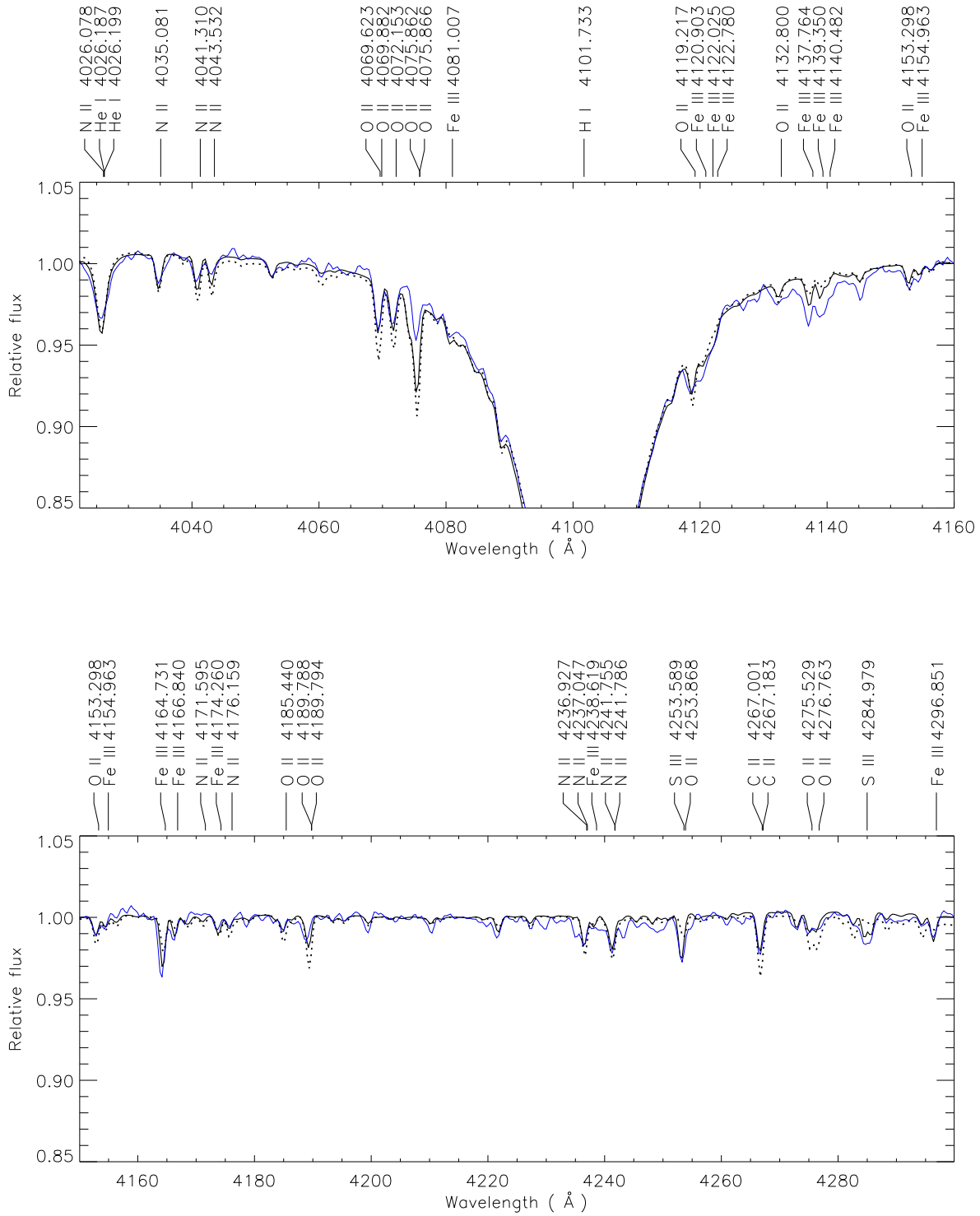


Figure 7. Detailed comparison of the observed MMT spectrum (blue line) with a synthetic spectrum (black line) having the abundances fine tuned in order to obtain a better match. The model atmosphere used for generating the synthetic spectrum has the parameters found by the fitting procedure of the MMT spectrum : $T_{\text{eff}} = 29,674$ K, $\log g = 5.43$ and $\log N(\text{He})/N(\text{H}) = -2.88$. The synthetic spectra obtained from the fitting procedure (in Fig 5a) is also shown (dotted line). The main absorption features are indicated with the name of the ion and the wavelength of the transition.

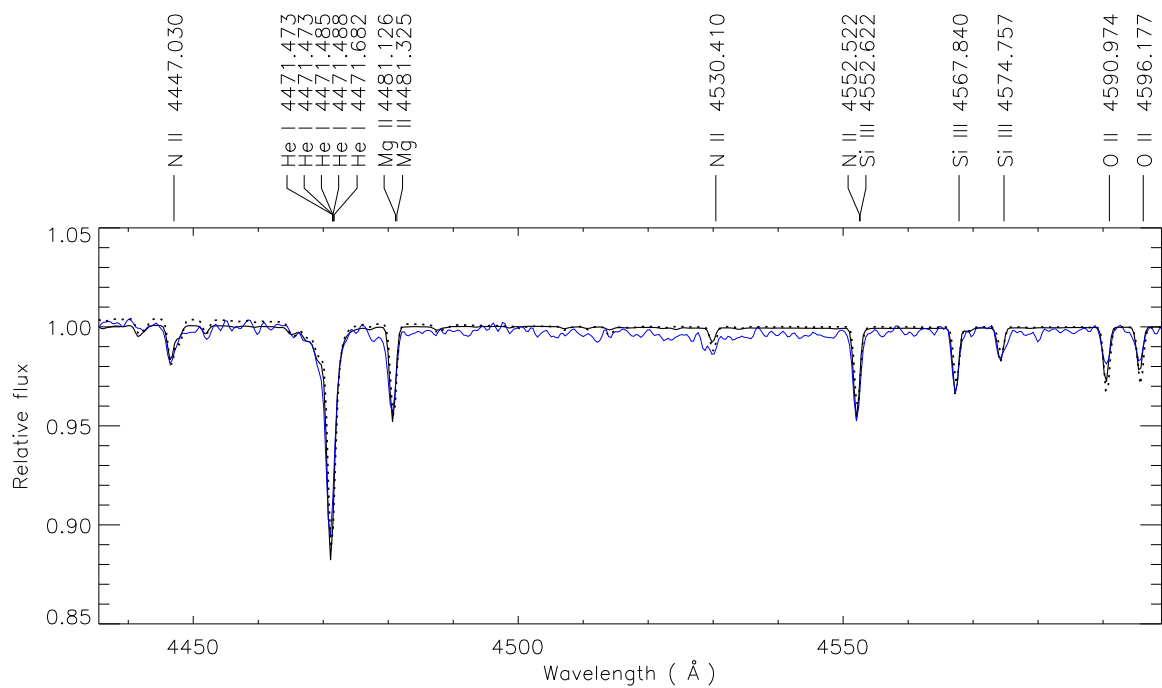
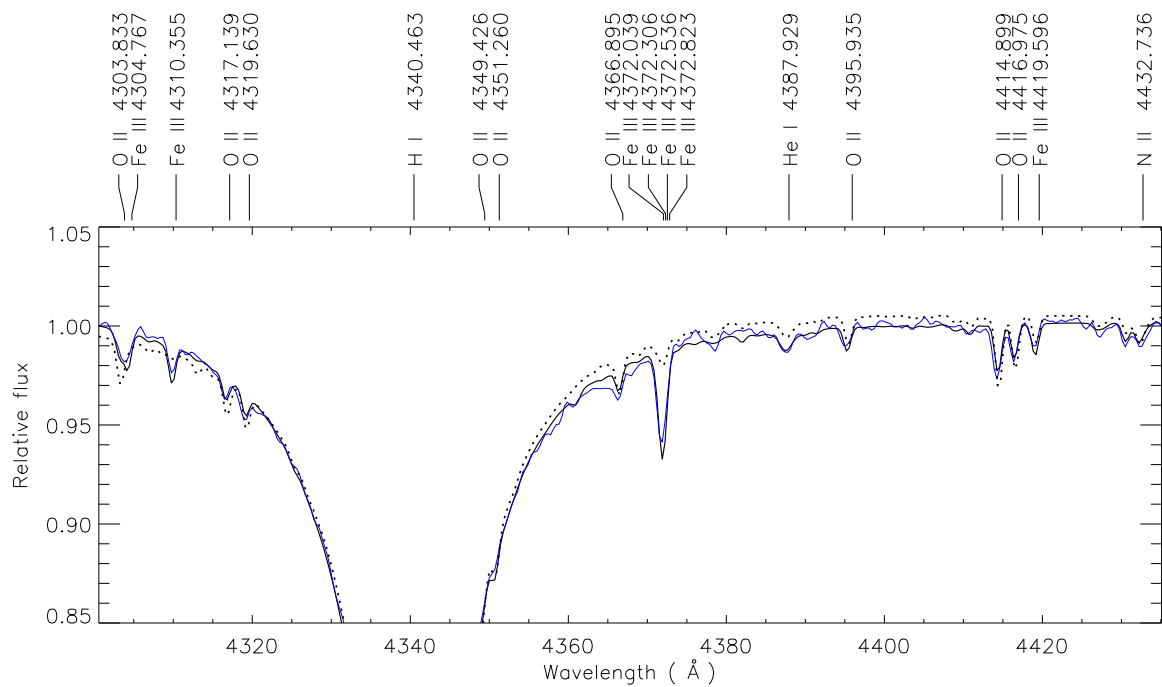


Figure 7. Continued.

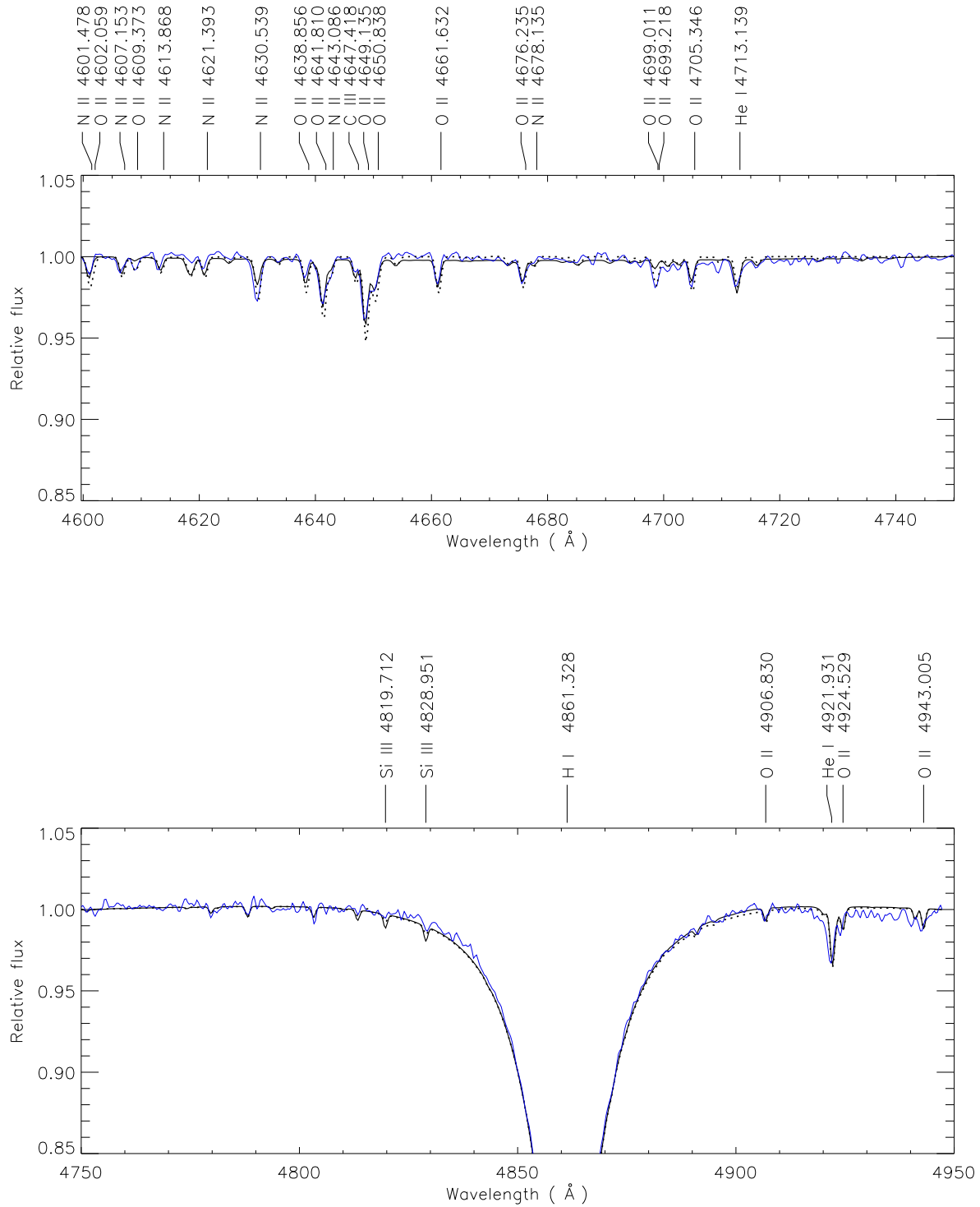


Figure 7. Continued. There is an offset of the wavelengths from He I λ 4922 until the end of the spectrum, probably due to the wavelength calibration that is not exactly right at the very end of the spectrum.

match when changing the abundance in the synthetic spectra or in the model atmosphere directly. After a thorough inspection of the synthetic spectra, it appears that some emission was occurring in a few iron lines, an unexpected and certainly unrealistic result. The two most problematic sets of lines (the complex around 4372 Å and Fe III λ 4310.355) originate from within two specific superlevels, and we suspect that there might be a problem with the populations of the different components of the superlevels. These components (within a given superlevel) are assumed to be in Boltzmann equilibrium with respect to each other. The solution we found to avoid this problem was to add iron in a synthetic spectrum computed from a model atmosphere that does not include iron. In this way, SYNSPEC computes the iron population in LTE and no strange emission occurs. When using these kind of spectra, we found a good match to the observed lines corresponding to an optimal iron abundance of $\log N(\text{Fe})/N(\text{H}) = -4.48$, which is very near the mean value obtained in Table 1.

Overall we can conclude that only minor adjustments were required in order to match in a better way the metallic lines featured in our MMT spectrum. Our new abundances for the seven species seen in this spectrum all agree very well with the previous measurements made in the past studies reported in Table 1.

3.6. Interstellar Reddening

The χ^2 method that we have used to derive the atmospheric parameters of Feige 48 is not sensitive to the presence of interstellar reddening since it relies on the (simultaneous) fits of the line profiles of hydrogen and helium, and not on the overall flux-calibrated spectrum. Nevertheless, it is instructive to verify after the fact if reddening is indeed small, as assumed by construction in our χ^2 approach.

From our best-fitting synthetic spectrum, characterized by $T_{\text{eff}} = 29,850$ K, $\log g = 5.46$, $\log N(\text{He})/N(\text{H}) = -2.88$, and the metallicity given in the 7th column of Table 1, we derive an unreddened color index $(B - V)_0 = -0.255$. In comparison, the best available UBV photometry on Feige 48, that of Bern & Wramdemark (1973), gives $V = 13.480 \pm 0.026$, $B - V = -0.250 \pm 0.013$, and $U - B = -1.030 \pm 0.017$. Neglecting the uncertainties on the model color index, this immediately leads to a reddening index of $E(B - V) = 0.005 \pm 0.013$, which is indeed quite low.

An independent check on that result is provided by the use of the Strömgren photometry of Wesemael et al. (1992) which gives, for Feige 48, $V = y = 13.456 \pm 0.029$, $b - y = -0.116 \pm 0.017$, $u - b = -0.162 \pm 0.018$, and $m_1 = 0.086 \pm 0.018$. With the help of the relation $E(b - y) = 0.642 E(B - V)$ – which can be derived from the equations given in Seaton (1979) – and the unreddened model value of $(b - y)_0 = -0.123$, we find a reddening index of $E(B - V) = 0.011 \pm 0.036$, less accurate but entirely compatible with our first estimate.

4. CONCLUSION

As part of an ongoing major effort to exploit fully the asteroseismic potential of Feige 48 (a rare bright rapid pulsator part of a close binary system), our work aimed at obtaining the most accurate atmospheric parameters

possible for this sdB star. To achieve that goal, we analyzed four time-averaged optical spectra of this star — three of them having exceptionally high S/N — with state-of-the-art NLTE line-blanketed model atmospheres including the eight most abundant metallic species observed in the star’s atmosphere, namely, C, N, O, Ne, Mg, Si, Fe, and Ni. In comparison, previous atmospheric studies of Feige 48 were based on either line-blanketed LTE models with arbitrary metallicities or metal-free LTE and NLTE models.

Our final adopted parameters are the weighted mean of the solutions found with the different spectra: $T_{\text{eff}} = 29,850 \pm 60$ K, $\log g = 5.46 \pm 0.01$, and $\log N(\text{He})/N(\text{H}) = -2.88 \pm 0.02$, with the quoted uncertainties measuring only the quality of the spectral fits. A similar analysis made, this time, with more classical metal-free, H,He NLTE models led to very similar atmospheric parameters as indicated in Table 3. This demonstrates that the effects of combining the NLTE approach with metal line blanketing are not very large in the atmosphere of Feige 48. As depicted in Figure 4, part of this is accidental and specific to this particular star. Presumably, this coincidence explains why our derived parameters agree rather well with previous estimates based on less sophisticated models, implying that the current estimations of the atmospheric parameters of Feige 48 are reliable and sound. This is a good thing, particularly from an asteroseismological point of view, because it means that the spectroscopic constraints to be used in seismic studies, including past efforts, can be trusted.

During our investigations, we noticed a slight, but possibly significant systematic trend suggesting an increase of both the derived effective temperature and the surface gravity with decreasing resolution (from 1.0 to 8.7 Å in our data), while the helium abundance appeared to be insensitive. The overall differences are relatively small, ~ 600 K and ~ 0.09 dex, but the trend is seen in the fits carried out with both the metal-free and the line-blanketed grids. This is the first time we observe this effect in a sdB star, possibly because we had at our disposal exceptionally high S/N spectra. Geier et al. (2013) investigated the differences in effective parameters derived from medium resolution spectra and high-resolution echelle ones, they found the averages of the shifts to be $\Delta T_{\text{eff}} \simeq 1100$ K and $\Delta \log g \simeq 0.12$ and no systematic trend was seen. The differences we found for Feige 48 are consistent with these values. We also found that for the lower resolution spectra (PB6 and BG9), changing the spectral range of the fit leads to, within the fitting errors, the same estimates of the derived parameters and, thus, no observable systematic effects.

We also inspected the effects that the various metallic elements considered in the NLTE models have on the atmospheric structure. In the specific case of the models computed for Feige 48, the temperature in the outermost atmospheric layers is highly sensitive to the presence of the light metals, while the influence of iron and nickel is mostly confined to layers deeper than $\log m \simeq -3.0$. The actual amount of nickel present in the atmosphere of the star, $\log N(\text{Ni})/N(\text{H}) = -5.31$, does not produce a significant added effect on the temperature structure modified already by the presence of the light metals and iron.

As a consistency check, we fitted the only He II spectral feature that we could find in the spectrum of Feige 48 which, otherwise, contains only H I and He I lines. And indeed, through the MAST archives, we retrieved and fitted the weak He II line at 1640 Å present in the STIS spectrum of Feige 48. This was done in terms of effective temperature and surface gravity only (the helium abundance being fixed), leading to the independent estimates of $T_{\text{eff}} = 30,450 \pm 930$ K and $\log g = 5.43 \pm 0.30$, fully consistent with our values derived from the optical data.

Our best data set was the MMT spectrum, characterized by the relatively high resolution of 1.0 Å over a spectral range 4000–4950 Å, and the very high value of S/N \simeq 460. This particular spectrum shows a host of distinct metallic lines that could be examined in details. With the initial metallicity specified as in Table 1, a good agreement was obtained between the observed and predicted metal lines as can be seen in Figure 5a. However, a distinct improvement was reached when slightly adjusting the individual metal abundances as was done in Subsection 3.5. The detailed results are presented in the series of Figure 7.

The atmospheric parameters derived here for Feige 48 will provide an essential ingredient in the upcoming new seismic analysis of that star, which will be based on the recent extensive photometric campaign that has revealed some 46 pulsation modes compared to the 9 modes previously known (Green et al., in preparation). Likewise, these estimates form the basis of the method that is used to exploit the signature that the degree index ℓ of a pulsation mode leaves on the wavelength-amplitude relationship (see, e.g., Randall et al. 2005). In the specific case of Feige 48, Fontaine & Chayer (2006) and Quirion et al. (2010) have presented preliminary efforts to exploit this signature by comparing optical with FUV amplitudes, and these certainly deserves to be pushed further on the basis of our improved determinations of the atmospheric parameters of that pulsator. A priori mode identification can be extremely useful in the search for an optimal seismic model in parameter space (Van Grootel et al. 2008).

This work was supported in part by the Natural Sciences and Engineering Research Council of Canada through a doctoral fellowship awarded to M.L. and through a research grant awarded to G.F. The latter also acknowledges the contribution of the Canada Research Chair Program. We are also most grateful to Pierre Bergeron for providing us with a spectrum of Feige 48.

REFERENCES

- Bern, K. & Wramdemark, S. 1973, *Lowell Observatory Bulletin*, 8, 1
- Blanchette, J.-P., Chayer, P., Wesemael, F., Fontaine, G., Fontaine, M., Dupuis, J., Kruk, J. W., & Green, E. M. 2008, *ApJ*, 678, 1329
- Brassard, P., Fontaine, G., Billères, M., Charpinet, S., Liebert, J., & Saffer, R. A. 2001, *ApJ*, 563, 1013
- Brassard, P., Fontaine, G., Chayer, P., & Green, E. M. 2010, in *American Institute of Physics Conference Series*, Vol. 1273, American Institute of Physics Conference Series, ed. K. Werner & T. Rauch, 259–262
- Charpinet, S., Fontaine, G., Brassard, P., Billères, M., Green, E. M., & Chayer, P. 2005a, *A&A*, 443, 251
- Charpinet, S., Fontaine, G., Brassard, P., Chayer, P., Rogers, F. J., Iglesias, C. A., & Dorman, B. 1997, *ApJ*, 483, L123
- Charpinet, S., Fontaine, G., Brassard, P., & Dorman, B. 1996, *ApJ*, 471, L103
- Charpinet, S., Fontaine, G., Brassard, P., Green, E. M., & Chayer, P. 2005b, *A&A*, 437, 575
- Charpinet, S., Van Grootel, V., Brassard, P., Fontaine, G., Green, E. M., & Randall, S. K. 2013, in *Astronomical Physical Journal Web of Conferences*, Vol. 43, European Physical Journal Web of Conferences, 4005
- Chayer, P., Fontaine, G., Fontaine, M., Lamontagne, R., Wesemael, F., Dupuis, J., Heber, U., Napiwotzki, R., & Moehler, S. 2004, *Ap&SS*, 291, 359
- Fontaine, G., Brassard, P., Charpinet, S., Green, E. M., Chayer, P., Billères, M., & Randall, S. K. 2003, *ApJ*, 597, 518
- Fontaine, G. & Chayer, P. 2006, in *Astronomical Society of the Pacific Conference Series*, Vol. 348, *Astrophysics in the Far Ultraviolet: Five Years of Discovery with FUSE*, ed. G. Sonneborn, H. W. Moos, & B.-G. Andersson, 181
- Geier, S. 2013, *A&A*, 549, A110
- Geier, S., Heber, U., Edelmann, H., Morales-Rueda, L., Kilkenny, D., O’Donoghue, D., Marsh, T. R., & Copperwheat, C. 2013, *A&A*, 557, A122
- Green, E. M., Fontaine, G., Reed, M. D., Callera, K., Seitzzahl, I. R., White, B. A., Hyde, E. A., Østensen, R., Cordes, O., Brassard, P., Falter, S., Jeffery, E. J., Dreizler, S., Schuh, S. L., Giovanni, M., Jeffery, E. J., Dreizler, S., Schuh, S. L., Giovanni, M., Edelmann, H., Rigby, J., & Bronowska, A. 2003, *ApJ*, 583, L31
- Heber, U. 2009, *ARA&A*, 47, 211
- Heber, U., Reid, I. N., & Werner, K. 2000, *A&A*, 363, 198
- Kilkenny, D., Fontaine, G., Green, E. M., & Schuh, S. 2010, *Information Bulletin on Variable Stars*, 5927, 1
- Kilkenny, D., Koen, C., O’Donoghue, D., & Stobie, R. S. 1997, *MNRAS*, 285, 640
- Koen, C., Kilkenny, D., O’Donoghue, D., van Wyk, F., & Stobie, R. S. 1997, *MNRAS*, 285, 645
- Koen, C., O’Donoghue, D., Pollacco, D. L., & Nitta, A. 1998, *MNRAS*, 300, 1105
- Lanz, T. & Hubeny, I. 1995, *ApJ*, 439, 905
- , 2003a, *ApJS*, 146, 417
- Lanz, T. & Hubeny, I. 2003b, in *Astronomical Society of the Pacific Conference Series*, Vol. 288, *Stellar Atmosphere Modeling*, ed. I. Hubeny, D. Mihalas, & K. Werner, 117
- , 2007, *ApJS*, 169, 83
- Latour, M., Fontaine, G., Brassard, P., Green, E. M., Chayer, P., & Randall, S. K. 2011, *ApJ*, 733, 100
- Latour, M., Fontaine, G., Chayer, P., & Brassard, P. 2013, *ApJ*, 773, 84
- Napiwotzki, R. 1997, *A&A*, 322, 256
- Németh, P., Kawka, A., & Vennes, S. 2012, *MNRAS*, 427, 2180
- O’Donoghue, D., Lynas-Gray, A. E., Kilkenny, D., Stobie, R. S., & Koen, C. 1997, *MNRAS*, 285, 657
- O’Toole, S. J. & Heber, U. 2006, *A&A*, 452, 579
- O’Toole, S. J., Heber, U., & Benjamin, R. A. 2004, *A&A*, 422, 1053
- Quirion, P.-O., Podmore, H., & Dupuis, J. 2010, in *American Institute of Physics Conference Series*, Vol. 1273, *American Institute of Physics Conference Series*, ed. K. Werner & T. Rauch, 554–557
- Randall, S. K., Fontaine, G., Brassard, P., & Bergeron, P. 2005, *ApJS*, 161, 456
- Reed, M. D., Kawaler, S. D., Zola, S., Jiang, X. J., & et al. 2004, *MNRAS*, 348, 1164
- Saffer, R. A., Bergeron, P., Koester, D., & Liebert, J. 1994, *ApJ*, 432, 351
- Seaton, M. J. 1979, *MNRAS*, 187, 73P
- Stobie, R. S., Kawaler, S. D., Kilkenny, D., O’Donoghue, D., & Koen, C. 1997, *MNRAS*, 285, 651
- Van Grootel, V., Charpinet, S., Fontaine, G., & Brassard, P. 2008, *A&A*, 483, 875
- Wesemael, F., Fontaine, G., Bergeron, P., Lamontagne, R., & Green, R. F. 1992, *AJ*, 104, 203